Journal of Catalysis **197,** 113–122 (2001)
doi:10.1006/jcat.2000.3069, available online at http://www.idealibrary.com on IDEAL®

CO Oxidation over Supported Gold Catalysts—"Inert" and "Active" Support Materials and Their Role for the Oxygen Supply during Reaction

Markus M. Schubert,*,[1] Stefan Hackenberg,* Andre C. van Veen,† Martin Muhler,† Vojtech Plzak,‡ and R. Jürgen Behm*

*Abteilung Oberflächenchemie und Katalyse, Universität Ulm, D-89069 Ulm, Germany; †Lehrstuhl für Technische Chemie, Ruhr-Universität Bochum, D-44780 Bochum, Germany; and ‡Zentrum für Sonnenenergie- und Wasserstoff-Forschung (ZSW), Helmholtzstrasse 8, D-89081 Ulm, Germany

Received May 25, 2000; revised September 5, 2000; accepted September 5, 2000

A thorough comparison of gold catalysts on different support materials as well as activity measurements for Au on mixed oxides ($Au/Fe_2O_3 \cdot MgO$) reveal enhanced CO oxidation rates for a group of "active" support materials (Fe_2O_3, TiO_2, NiO_x, CoO_x). For Au/Fe_2O_3, it is shown that large amounts of oxygen can adsorb on the support, which most likely represents the oxygen supply during reaction. The high mobility of these oxygen species and the absence of oxygen scrambling with labeled $^{36}O_2$ in pulse experiments strongly suggest the adsorption in a molecular form on the iron oxide support. From the absence of the doubly marked product $C^{18}O^{18}O$, reaction schemes via a carbonate-like intermediate or transition-state can be ruled out. For Au catalysts supported on active materials, the dominant reaction pathway is concluded to involve adsorption of a mobile, molecular oxygen species on the support, dissociation at the interface, and reaction on the gold particles and/or at the interface with CO adsorbed on the gold. The facile supply with reactive oxygen, via the support, serves as a probable explanation for the observed independence of the turnover frequency from the Au particle size on these catalysts, while for Au supported on inert materials, where the oxygen supply most likely proceeds via direct dissociative adsorption on the Au particles, the size of the latter plays a decisive role.

Key Words: **CO oxidation; supported gold catalysts; Au/Fe_2O_3; oxygen adsorption; reaction mechanism; support effects; isotope labeling; TAP.**

I. INTRODUCTION

Gold has long been disregarded for catalytic purposes due to the inert nature of massive gold. However, when it is supported on metal oxides in a highly dispersed state, it exhibits a surprisingly high activity for several reactions, including CO oxidation ((1–3) and references therein). The striking difference between the catalytic behavior of massive Au samples and supported Au catalysts has prompted numerous studies on the underlying physical origin, which came to partly contradictory results. In particular the role of the support for the catalytic reaction is still under discussion. Stimulated by the high activity observed for a Au/α-Fe_2O_3 sample for the preferential CO oxidation in H_2-rich gas (PROX) in an earlier study (4)—the latter reaction is applied for the CO removal from feed gas streams for polymer electrolyte membrane (PEM) fuel cells—we extended our studies to mechanistic aspects of the CO oxidation reaction on supported Au catalyst, focusing on the role of the substrate and on the oxygen supply.

Before presenting and discussing the experimental results we will briefly summarize the previous findings. For massive Au samples it is well known that (i) CO reversibly adsorbs at low temperatures ($T < 150$ K) (5), or, in dynamic equilibrium at sufficiently high partial pressures, also around room temperature (6), (ii) dissociative adsorption of oxygen at temperatures below 400°C is strongly hindered by a high dissociation barrier (7), which is attributed to a weak coupling to the Au substrate due to the filled *d*-states (8), and (iii) CO oxidation takes place readily only when oxygen is provided in atomic form (7, 9, 10). The reverse process, desorption of atomically adsorbed oxygen, is likewise strongly activated by activation barriers in the range of 100–150 kJ/mol (10–12).

For supported Au catalysts there is general agreement that CO is adsorbed on the gold particles, as evidenced by an infrared band at ~2110 cm^{-1} which is not present, e.g., on pure Fe_2O_3, and that the CO oxidation reaction follows a scheme where both reactants are bound to the surface of the catalyst (13–20). Highly controversial, however, are the mechanisms for oxygen adsorption and activation which are required to explain the activity for CO oxidation and which contrast the inhibited oxygen dissociation on single crystals.

[1] Present address: Laboratory for Technical Chemistry, Swiss Federal Institute of Technology, ETH-Zentrum, CH-8092 Zürich, Switzerland. E-mail: markus.schubert@tech.chem.ethz.ch.

0021-9517/01 $35.00

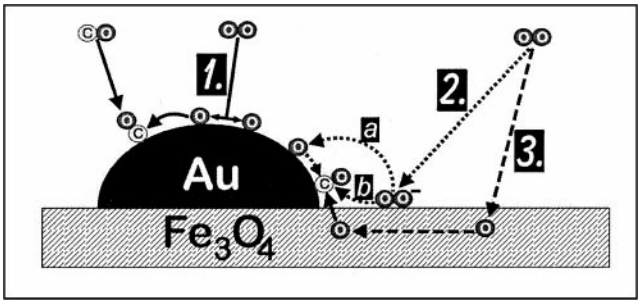

FIG. 1. Possible reaction schemes for the CO oxidation reaction over supported Au catalysts (here, Au/Fe_3O_4).

Several models have been proposed to resolve this controversy. For a better overview the most frequently proposed mechanisms for oxygen adsorption on supported Au particles are visualized in Fig. 1.

The first model (No. 1) assumes that oxygen adsorption proceeds directly on the gold particles (2, 10, 21). The oxygen bond cleavage was suspected to be induced either by the formation of a four-center surface complex including CO and O_2 being adsorbed on a common Au site, which would form a labile precursor state (2) or to occur on metal surface defect sites (22, 23) or on small, flat-shaped particles with a different electronic structure (10, 21), respectively. For this model the role of the support material is limited to the stabilization of very small gold particles and/or particles with highly reactive gold sites or crystallite faces.

In the other models, the oxygen adsorption is believed to occur on the support (or at the metal–support interface) (15, 18, 19, 24–26), possibly on oxygen vacancies (17, 26), which should be present on semiconductor materials such as TiO_2, Fe_3O_4, or ZnO (27), especially in the proximity of the Au particles as a consequence of the Schottky junction at the metal–semiconductor interface (28). Iwasawa and coworkers suggested adsorption of molecular superoxide oxygen species (O_2^-; reaction pathway No. 2 in Fig. 1), which were evidenced by ESR measurements (17, 24, 26). They did not specify, however, whether these would dissociate at the interface to give O_{ad} (corresponding to pathway No. 2a) or react directly with adsorbed CO (pathway No. 2b). The latter would most plausibly include a carbonate-like transition state or intermediate (16). In the last reaction pathway proposed previously (No. 3 in Fig. 1) it is assumed that oxygen adsorbing on the support dissociates immediately, producing lattice oxygen, which can subsequently react at the interface or after a spillover of oxygen to the gold metal (15, 19).

In the following we will, after a brief description of the experimental setup and procedures, first present activity measurements on various Au catalysts with different oxide supports, which will be discussed in comparison with similar measurements from previous studies on CO oxidation. This will show that active supports such as Fe_2O_3 enhance the activity of gold catalysts significantly. To further elucidate the role of the support, the next section presents similar measurements on a series of $Au/Fe_2O_3 \cdot MgO$ catalysts with varying support composition. Since the two components can be considered as representative for a nonactive ("inert") and an active support, this represents a well-defined model system with constant preparation conditions, which spans the entire range from active to inert support materials. The last two sections focus on an exemplary investigation of the oxygen adsorption characteristics on $Au/\alpha\text{-}Fe_2O_3$. Time resolved CO/O_{ad} titration experiments will be shown which demonstrate that iron oxide is able to adsorb large quantities of highly mobile oxygen species that can react with CO. Additional mechanistic information comes from experiments with isotope labeled $^{36}O_2$. On the basis of these results a comprehensive mechanistic picture for the oxygen supply during CO oxidation over supported gold catalysts is derived.

II. EXPERIMENTAL

The gold catalysts were prepared either by deposition-precipitation ($Au/\alpha\text{-}Fe_2O_3$) and by coprecipitation ($Au/\alpha\text{-}Fe_2O_3$, Au/NiO_x, $Au/Mg(OH)_2$, and Au/MgO, resp., $Au/Fe_2O_3 \cdot MgO$) in close accordance to the routes described in Refs. (16, 29) or by impregnating the support materials (Au/Al_2O_3, Au/TiO_2, Au/CoO_x) with $HAuCl_4$ at 60°C near the isoelectric point of the corresponding oxide. The actual loading of each sample was checked by AAS. For comparison a commercial $Pt/\gamma\text{-}Al_2O_3$ catalyst (Degussa F 213 XR/D) with a metal loading of 0.5 wt% was employed. Metal particle sizes and particle size distributions were determined by TEM (Au/TiO_2, Au/CoO_x, Au/NiO_x, $Pt/\gamma\text{-}Al_2O_3$) or by XRD via the Scherrer equation.

Prior to reaction the Au catalysts were calcined in 10 kPa O_2 in N_2 (30 min; 20 Nml/min) at 400°C (300°C for $Au/Mg(OH)_2$). The $Pt/\gamma\text{-}Al_2O_3$ catalyst was additionally reduced in flowing hydrogen (both 20 Nml/min, 30 min at 350°C), resulting in an average particle size of ca. 2.3 ± 0.6 nm (TEM), which corresponds to a dispersion of ca. 40%. (All gas flows are in units of Normmilliliter (Nml), i.e., related to standard conditions of 0°C and 103.1 kPa.)

The activity measurements and titration experiments were carried out in a tubular reactor (i.d. 4 mm), which contained approximately 100 mg of powder fixed by quartz wool plugs. In order to guarantee differential conditions (conversion <20%), the catalysts were diluted with $\alpha\text{-}Al_2O_3$. The gas mixture leaving the reactor tube was analyzed by a GC (Chrompack CP9001), equipped with widebore capillary columns (Poraplot U and Molsieve 5 Å; Chrompack) and thermal conductivity detectors. The rates for CO oxidation ($mol_{CO}/g_{Au} \cdot s$) and the corresponding turnover frequencies, TOF (s^{-1}), which are normalized to the number of exposed metal surface atoms, were

determined in an atmosphere of simulated methanol reformer gas, which contained 1 kPa CO in 75 kPa H_2 and balance N_2. O_2 (1 kPa) was added for the oxidation reaction. The additional presence of hydrogen was shown to hardly affect the CO oxidation reaction (20, 30) and therefore does not need to be regarded for the following mechanistic considerations. The gases N_2 (6.0), H_2 (5.0), 2% CO (4.7) in H_2 (5.6) and 10% O_2 (5.0) in N_2 (5.0, CO-free) were supplied by Linde, Messer Griesheim and MTI.

For the titration experiments, on-line analysis was performed with an IMR-MS (ion-molecule-reaction mass spectrometer; Atomika), which allows detection of CO and CO_2 in a nitrogen matrix without interference problems. The gate time for analysis was 0.2 s for each detected component (O_2, CO_2, CO, Kr, Xe), equivalent to the acquisition of 1 data point per second. For quantitative analysis all signals were calibrated with the help of reference gases with known composition.

The isotope/pulse studies were performed in a TAP reactor (temporary analysis of products; model 1b, equipped with a high-pressure assembly). A detailed description of the typical TAP setup and the employed reactor type, which contained about 50 mg catalyst powder, is found in Ref. (31). All experiments were performed in the vacuum-flow mode (i.e., with vacuum applied to the exit), which is characterized by a short contact time for the reactants (incoming reactant flow ca. 1 Nml/min). For the present investigations we admitted pulses of isotope labeled $^{36}O_2$ (Cambridge Isotope Laboratories; ca. 95% ^{18}O; diluted with Argon 1 : 5; $\sim 2 \times 10^{15}$ molecules/pulse) to a continuously flowing reaction mixture for the selective CO oxidation (ca. 1.7% CO and O_2; 75% H_2, balance Ne). Under these conditions the catalyst is probed in the active state of the selective reaction. However, it is not possible to determine rate constants by conventional methods due to the viscous flow applied.

III. RESULTS AND DISCUSSION

a. Comparison of Different Support Materials

First we want to clarify how the choice of the support material influences the activity of a gold catalyst for CO oxidation. The results of a series of activity measurements on Au catalysts on different metal oxides are listed in Table 1 (all data taken after 2 h on-stream). These data allow a clear division of the catalysts into two different categories: On the one hand there are catalysts that exhibit a lower, but still considerable activity, as evidenced by their TOFs. Characteristic for these catalysts are their basically irreducible oxide supports such as Al_2O_3 and MgO. These materials have a low ability to adsorb or store oxygen at these low temperatures. On the other side are catalysts which are supported on reducible transition metal oxides, such as Fe_2O_3, NiO_x, CoO_x, or TiO_2. They exhibit a superior activity, higher by up to one order of magnitude. The existence of such a "support effect" was, e.g., also recognized by Grunwaldt *et al*., who found the activity of a titania supported sample to be one order of magnitude higher than that of a Au/ZrO_2 catalysts (32). Likewise, Bollinger and Vannice demonstrated that a titania coating added subsequently could increase the activity of a gold powder considerably (18).

For comparison data from selected other studies have been included in Table 1 as well (rates and TOFs are extrapolated to our standard reaction temperature of 80°C). These results clearly underline our above division of oxide supported Au catalysts into two different groups.

The influence of the support material points to differences also in the reaction mechanism. For "inert" support materials it is a logical consequence that oxygen adsorption and dissociation must be possible on the gold metal (corresponding to pathway 1 in Fig. 1), whereas for "active" metal oxides, participation of the support in the CO reaction may explain the superior activities of the corresponding catalysts. Moreover, for inert supports the activity seems to depend very critically on the diameter of the gold particles, and only extremely small particles (2 nm and below) yield highly active samples (see Table 1). This explains also why our own catalysts (Au/γ-Al_2O_3 or Au/MgO and $Au/Mg(OH)_2$, resp.) turned out to be slightly less reactive than those in the previous studies listed in Table 1. Such a dependence on particle size for catalysts with an inert support was also demonstrated by Okumura *et al*. for Au/SiO_2 (33), as well as by Cunningham *et al*. for the $Au/Mg(OH)_2$ system (34). The increasing TOF with smaller particle size was explained by an enhanced dissociative adsorption of oxygen on small gold particles, due to a higher density of reactive defect sites (edge, kink, or step sites) (23, 35) or a gradual change in the electronic structure at decreasing size (10, 21, 34).

For the second group, where active oxides such as Fe_2O_3 or TiO_2 are employed as support, the size of the gold particles seems to play only a secondary role. Even catalysts with gold particles as large as 12 (Au/Fe_2O_3) or 30 nm (Au/TiO_2) still exhibit a TOF comparable to those with small Au particle sizes (see Table 1). For our own Au/α-Fe_2O_3 catalysts we noted a constant, high TOF within a tolerance of $\pm 50\%$ for Au particles ranging from 2.8 up to 11 nm, which corroborates these results (30, 36). It should be mentioned that this finding contradicts recent reports for gold particles deposited on a $TiO_2(110)$ single crystal and for disperse Au/TiO_2 catalysts where a decrease of the TOF at increasing particle size has been noticed (10, 21). For the former model system, a possible explanation for this apparent discrepancy is the very high "metal loading," where the metal covers up to 75% of the TiO_2 surface (10) and the mechanism proposed below may no longer hold true; in the latter case it has to be noted that the difference is mainly caused by the much lower TOF of the samples with larger particles sizes

TABLE 1

Comparison of Our Kinetic Data for the CO Oxidation over Supported Au Catalysts (Data Taken in Simulated Methanol Reformate after 2 h on Stream) with Values Calculated from Selected Other Studies (Rates Extrapolated to Our Reaction Temperature of 80°C)

Catalyst	Prep.[a]	d_{Au} [nm]	p(CO) [kPa]	$p(O_2)$ [kPa]	r ($\times 10^4$) [$mol_{CO}/g_{Au} \cdot s$]	TOF[b] [s^{-1}]	E_a [kJ/mol]	Ref.
Au/Fe_2O_3	DP	2.3–7	1	1	39[c]	1.3–3.0	29	This work
	—	—	1	20	74	2.9–6.7	—	This work[d]
	CP	5.5–7	1	1	43[c]	3.2–3.4		This work
	DP	3.6	0.2–6[e]	1–20[e]	13	0.7	35	16
	IMP	~4	1	10	11–12[f]	0.55–0.65		46
	DP[g]	12	1	20	6.4	1.0	21	24, 47
Au/NiO_x	CP	3.2 ± 1.0	1	1	20	1.3		This work
Au/CoO_x	IMP	3.4 ± 1.4	1	1	22	1.8		This work
Au/TiO_x	IMP	2.4 ± 0.7	1	1	33 (51[h])	1.6 (2.5[h])	21	This work
	IMP	33	4.9	4.9	8.1	4.5[i]	29	18
	DP	2.9	1	20	33	1.3	27	22
	DP[g]	3	1	20	20[j,k]	0.8		24, 48
	DP[g]	30	1	20	2.0	0.7	12	24, 47
$Au/Mg(OH)_2$	CP	<4	1	1	13	0.5–0.9		This work
	DP	0.6–1.2	1	20	>51[l]	>1.2		34
Au/MgO	CP	6.0	1	1	3.8	0.3		This work
Au/Al_2O_3	IMP	4.4	1	1	6.0	0.35		This work
	DP	2.4	1	20	13	0.5	32	33
	CVD	3.5	1	20	7.6	0.35	36	33
Au/SiO_2	CVD	6.6	1	20	1.3	0.1	17	33
	DP	30	4.9	4.8	0.08	0.04	15	3
Au powder	—	20	1	20	~0.001[j]	$\sim 3 \times 10^{-4}$	~20[m]	16, 49

[a] DP, deposition–precipitation; CP, coprecipitation; IMP, impregnation; CVD, chemical vapor deposition.
[b] (Hemi-)spherical particles assumed, except where otherwise reported.
[c] Statistical average from all produced DP/CP catalysts.
[d] Extrapolated via O_2 reaction order of 0.27 (4).
[e] Reported reaction orders were zero.
[f] Extrapolated from $r = 1.4 \times 10^{-3}$ $mol/g_{Au} \cdot s$ at 90°C with $15 < Ea < 30$ kJ/mol.
[g] With phosphine-stabilized Au complex.
[h] After additional pretreatment in H_2 (250°C; 30 min); TGA indicates the formation of surface hydroxyl groups which appear to facilitate the CO oxidation, while the Au particles remain unchanged (XRD).
[i] Ca. 2.3 s^{-1}, when calculated for 1 kPa CO and $\lambda = 2$ with the reported reaction orders of 0.5 (CO) and 0.08 (O_2) at 30°C.
[j] Measured at high conversion.
[k] Extrapolated from $r = 9.6 \times 10^{-3}$ $mol/g_{Au} \cdot s$ at 28°C with $E_a = 12$ kJ/mol.
[l] Extrapolated from $r = 1.2 \times 10^{-4}$ $mol/g_{Au} \cdot s$ at −70°C with $E_a > 15$ kJ/mol.
[m] Activation energy estimated from conversion data.

(>4.6 nm diameter) and that these catalysts were prepared in a different way (photodeposition instead of deposition–precipitation), which is likely to cause differences also in the local structure and surface composition.

b. Activity Enhancement by Fe_2O_3

Because of the differences in the preparation procedures and reaction conditions for the various samples in Table 1 and since the extrapolation of the reaction rates to our operation temperature introduces additional uncertainties, further experimental evidence is required in order to corroborate the existence of a "support effect." For this purpose we investigated a series of identically prepared mixed-oxide supported catalyst ($Au/Fe_2O_3 \cdot MgO$) with varying compositions, where the two components are representative of an inert support (MgO) and active support (Fe_2O_3), respectively.

In Fig. 2 the reactivity (rate and TOF) of the $Au/Fe_2O_3 \cdot MgO$ catalysts is plotted as a function of the Mg content in the support (Figs. 2a and 2b). Although the catalysts were calcined as usual at 400°C prior to the reaction, the TOF in Fig. 2b is related to the number of exposed metal atoms after a calcination step at 600°C. The reason for this procedure is that after calcination at 400°C the samples in the mid-range of the concentrations of Mg were X-ray amorphous and a reasonable determination of the Au particle size by XRD and therefore of the TOF would not be possible. The progressing sintering of the gold clusters at 600°C enables a more precise determination of the particle size (Fig. 2c). It is assumed that the additional reduction of dispersion, caused by sintering between 400 and 600°C, is

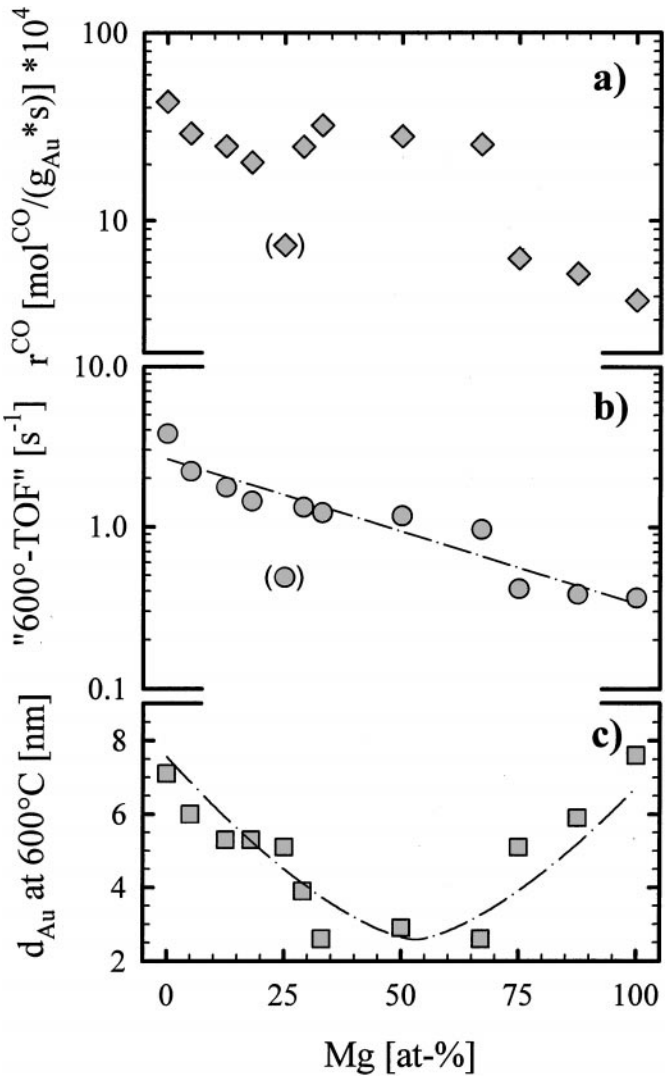

FIG. 2. (a) Rate, (b) turnover frequency for the CO oxidation in simulated methanol reformate (rate measured after calcination at 400°C but TOF is related to the dispersion after calcination at 600°C), and (c) Au particle diameter at 600°C (lower window) for $Au/Fe_2O_3 \cdot MgO$ mixed-oxide catalysts as a function of the Mg content in the support material.

rather similar for all support compositions, which was indeed confirmed by XRD-measurements for higher temperatures of up to 900°C. Nevertheless, despite possible errors in the mid-range of support compositions, the same decreasing trend for the TOF from lower to higher MgO content is also found when it is normalized to the dispersion after calcination at 400°C.

For the mid-range of the concentrations (25–80 at.%) MgO and Fe_2O_3 form a nonstoichiometric hydrotalcite-like precursor, named Pyroaurite ($Mg_{6-x}Fe_{2+x}CO_3(OH)_{16} \cdot 4.5H_2O$) (37), which incorporates the gold in its layered structure (interlayer spacing 2.3 nm (38)) after preparation. Pyroaurite decomposes in the temperature range between 320 and 380°C (just below the final calcination temperature) irreversibly to amorphous MgO and α-Fe_2O_3 according to XRD/TGA (Thermogravimetry) results (36). Therefore, the gold precursor is immobilized during the thermal reduction to Au^0 (>350°C; TGA results (36)), which obviously leads to the stabilization of very small gold particles in the mid-range of the concentrations of Mg. On the "Mg-rich" side as well as on the "Fe-rich" side, sintering is increasingly governed by the growth of the pure oxide components, resulting in larger gold particles (Fig. 2c).

The reactivity determined for the Mg-rich catalysts indeed decreases with increasing particle size, as would be predicted for an inert support material (The lines included in Fig. 2 are just to guide the eye and are not intended to imply any calculated dependencies). In the opposite direction with increasing amounts of Fe_2O_3, the TOF is, however, enhanced in spite of the growing Au particle size. This demonstrates that the increased CO oxidation rate indeed must be attributed to the presence of the iron oxide support, as was suggested above. (The sample with 25 at.% Mg, where the formation of pyroaurite is not yet observed, yielded an unexpectedly low activity–probably a consequence of a nonuniform gold distribution, with the major part attached to the magnesia after calcination. This was indicated by a very strong deactivation during time on-stream, which is typical for pure MgO-supported catalysts).

The increasing TOF with increasing amounts of Fe_2O_3, in spite of the larger gold particles, clearly demonstrates the existence of a "support effect," as was suggested above. For inert support materials the dependence for the TOF on the particle size diameter is related to the limiting role of the direct dissociative adsorption of oxygen on the gold particles. For gold catalysts supported on reducible transition metal oxides (TiO_2, Fe_2O_3, NiO_x, and probably also CoO_x); however, the superior activity and as well as the observed independence of the TOF from the particle size (Table 1, (36)) point to a different mechanism and nature of the rate-limiting step. Since CO adsorption on Au is unlikely to be affected by the substrate, dissociative adsorption of oxygen (activation energy for dissociation) and the actual reaction step (activation energy for reaction) remain as possibilities for a support-induced modification of the reaction rate. In particular, this possible involvement of the support in the oxygen supply for the reaction, shall be investigated in more detail in the following sections.

c. CO–O_2 Titration Experiments

In order to further investigate a possible participation of the iron oxide support in the oxygen supply, we concentrated on possible differences in the timescale for the CO_2 evolution and on the amount of reactant species that can be adsorbed on the catalyst. In these experiments, CO_2 evolution upon exposure to CO was followed both for freshly conditioned catalysts and for catalysts preexposed to oxygen. As had been demonstrated in similar experiments by Grass and Lintz, the response times differ significantly

depending on whether the preadsorbed species is very mobile and resides on the same substrate as the second reactant or not (39). This way they could demonstrate that on a Pt/SnO_2 catalyst, CO is exclusively bound to the metal particles whereas the oxygen also adsorbs (probably dissociatively) on the support material and reacts only after slow diffusion to the metal–support interface, possibly including a spillover process to the platinum surface.

Our titration experiments with preadsorbed oxygen were performed on Au/α-Fe_2O_3 at 80°C and, for comparison, on the pure α-Fe_2O_3 support as well as on a Pt/γ-Al_2O_3 catalyst (recorded at 150°C for the latter, so that the TOFs in idealized reformate would be of similar magnitude (40)). In the latter case, it is established that oxygen adsorbs exclusively (and dissociatively) on the metal particles (see, e.g., (41, 42) and references therein). Additional experiments on the freshly calcined materials without preexposure to oxygen allow conclusions on whether lattice oxygen from the support is involved in the reaction.

For the reference experiment on Pt/γ-Al_2O_3 (containing a total amount of 2.76 μmol Pt), the reactor was cooled down to 150°C after conditioning and then saturated with 10 kPa O_2 in N_2 for 10 min (20 Nml/min) and purged with nitrogen (20 Nml/min) for ca. 5 min in order to remove the residual gas-phase O_2. Subsequently, a stream of 2 kPa CO in N_2 (10 ml) was admitted and the CO_2 response recorded by IMR-MS on-line analysis. The resulting CO_2 peak (Fig. 3) shows its maximum at 1.67 min and is quite narrow (FWHM = 0.26 min) as would be expected for a fast reaction, which proceeds by direct adsorption and reaction on the metal surface. The slight off-set in the baseline after admission of the CO is caused by CO_2 and O_2 impurities in the feedstream and was corrected for integration. The calculated amount of adsorbed oxygen is ~1.3 μmol, which corresponds fairly well to the number of surface metal atoms (ca. 1.2 μmol).

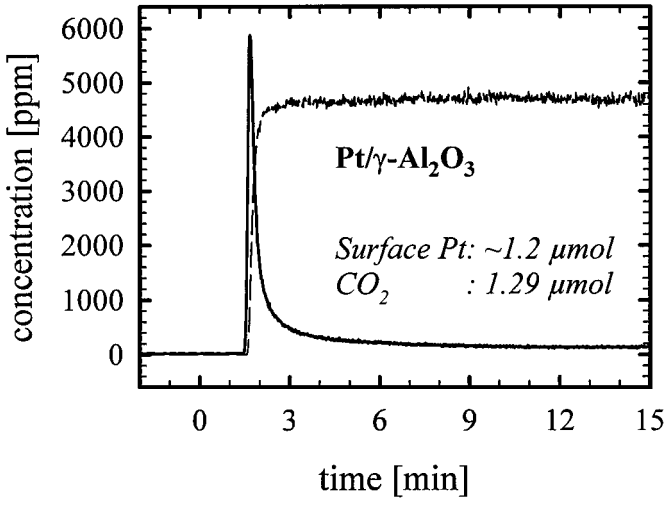

FIG. 3. CO_2 response (full line) for the reaction of preadsorbed oxygen with 2 kPa CO (dotted line) in N_2 over Pt/γ-Al_2O_3 at 150°C.

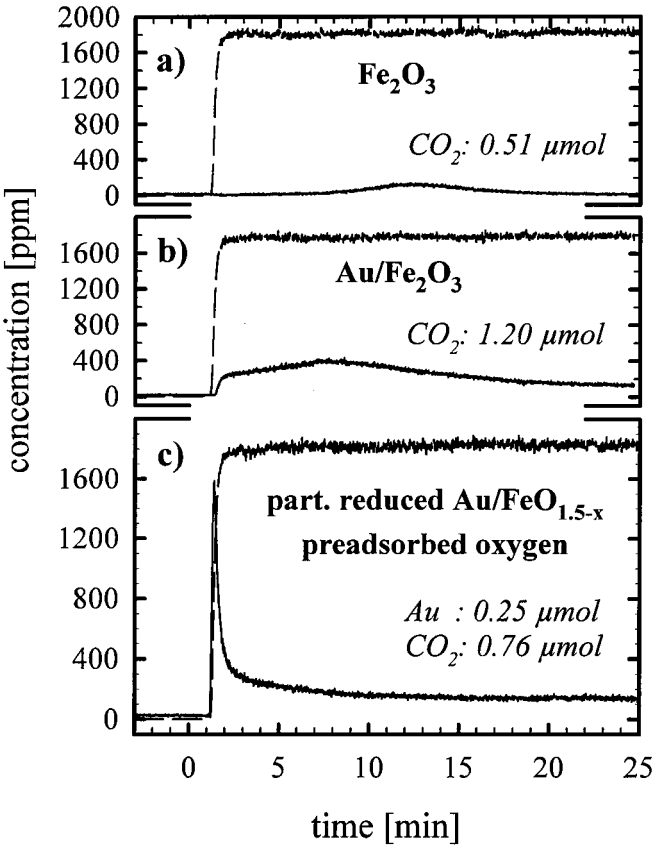

FIG. 4. CO_2 response (full lines) for the reaction of (a) freshly conditioned α-Fe_2O_3 with CO, (b) freshly conditioned Au/α-Fe_2O_3 with CO, (c) the subsequent reaction of preadsorbed oxygen over the partially reduced "$Au/FeO_{1.5-x}$" catalyst with CO (all reactions with 2 kPa CO (dotted line) in N_2 at 80°C).

For the measurements on the pure support, α-Fe_2O_3 (ca. 18 μmol Fe) was calcined at 400°C (30 min 10 kPa O_2 in N_2 at 20 Nml/min) and, after cooling down in pure nitrogen, titrated with 2 kPa CO in N_2 at our standard reaction temperature of 80°C without predosing additional oxygen (Fig. 4a). A small fraction of oxygen reacts after several minutes ($t_{max} \approx 12.3$ min; FWHM ≈ 6 min), presumably resulting from lattice oxygen liberated during the partial reduction of Fe_2O_3 to Fe_3O_4 (corresponding to ca. 17% conversion).

In a second run, after subsequently exposing the titrated sample to oxygen at 80°C, no further CO_2 evolution was detected upon switching back to the CO mixture, demonstrating that the partially reduced $FeO_{1.5-x}$ phase is stable to reoxidation under these conditions. Finally, the identical sequence, first titration of a freshly calcined sample and then, in a second run, after preadsorption of oxygen, was reproduced on the Au/α-Fe_2O_3 catalyst (ca. 17 μmol Fe; 0.25 μmol Au): After calcination, the catalyst was cooled

down to 80°C in N_2, and subsequently the CO mixture was admitted to the reactor (Fig. 4b). As for the pure support, we observed a rather broad CO_2 response, but this time the CO_2 production starts much faster (after ca. 1.7 min) and shows its maximum already at ~7.5 min (the absolute amount corresponds to a conversion of 43% Fe_2O_3 into Fe_3O_4), along with a pronounced tailing (FWHM ca. 10 min). It seems that the presence of gold strongly facilitates the reduction of the Fe_2O_3 support, which is attributed to the CO adsorption on the metal and subsequent reaction at the Au–Fe_2O_3 interface. In the second cycle (Fig. 4c) we preadsorbed oxygen (at 80°C; 20 Nml of 10 kPa O_2 in N_2 for 10 min) on this partially reduced catalyst, which should be chemically rather close to the state during PROX reaction in H_2-rich gas (Au/Fe_3O_4; determined by XRD/TGA (36)) and, after purging with nitrogen, switched back to the CO mixture. This time we observed an extremely sharp CO_2 peak ($t_{max} = 1.38$ min; FWHM = 0.38 min), very similar to the experiment with Pt/γ-Al_2O_3 (Fig. 3). There was no further slowly reacting oxygen species as for the freshly conditioned sample (Fig. 4b), similar to the observations after oxygen exposure on the partially reduced $FeO_{1.5-x}$ support.

This titration sequence could be reproduced repeatedly after the renewed preadsorption of oxygen, even when a reaction mixture of simulated methanol reformate was admitted to the reactor in the meantime in order to safely establish the typical steady state of the catalyst under reaction conditions. Due to its large amount (ca. 3 times more oxygen than Au atoms are available in total), the oxygen was not solely adsorbed on gold sites. Instead, large amounts must have been located on the support. From the very high reaction rate, we infer that this oxygen, which is believed to be the active species for the CO oxidation, is not lattice oxygen (O^{2-}), but rather a molecular oxygen species, probably in the form of superoxides (O_2^-), as were observed by Liu *et al*. in ESR measurements on a Au/TiO_2 catalyst (17). The participation of lattice oxygen, which caused the slow CO_2 responses on the freshly conditioned Au/α-Fe_2O_3 sample and on the pure α-Fe_2O_3 support, respectively, would have been characteristic for a reaction sequence including oxygen dissociation on the support and subsequent transport of atomic (lattice) oxygen to the gold–oxide interface via oxide lattice sites (pathway No. 3. in Fig. 1). This can therefore be excluded as a major reaction pathway. Molecular oxygen species adsorbed on the support plausibly explains both the fast reaction response (i.e., high mobility) as well as the large amount of preadsorbed oxygen available for the reaction.

The time-resolved titration experiments presented here provide clear evidence that the Fe_2O_3 support is involved in the CO oxidation reaction, acting as an oxygen supply which allows faster oxygen adsorption and thereby higher CO_2 formation rates; hence CO oxidation reaction over Au/α-Fe_2O_3 follows the reaction pathway 2 in Fig. 1.

d. Isotope Labeling Experiments

The above titration experiments, which were recorded sequentially—first conditioning or exposure to oxygen and then exposure to CO—provided valuable mechanistic information. Unfortunately, they may not be directly applicable to the reaction since under reaction conditions, the catalysts may be in a different state. Therefore it would be favorable to perform similar experiments on oxygen adsorption (and diffusion) and the subsequent reaction *during* CO oxidation under steady state conditions. This was attempted in the following isotope labeling experiments, where we introduced pulses of labeled oxygen ($^{36}O_2$) into a continuous gas stream for selective CO oxidation (containing $C^{16}O$ and $^{32}O_2$). These experiments should allow to distinguish between the reactions schemes 2a (oxygen dissociation prior to reaction) and 2b (reaction of molecular oxygen species with CO). Such kinds of experiments were already presented by Boccuzzi *et al*. (14, 43) and Liu *et al*.(17). Their experiments, however, were rather sensitive to readsorption effects, which play a much smaller role in the TAP reactor setup used in this study because of the much shorter contact times. It turned out, however, that even under these improved conditions the CO_2 response resulting from the $^{36}O_2$ pulses did not allow a clear interpretation due to the strong readsorption of the product CO_2 on the support material, which led to a significant broadening of the observed response signal (see inset in Fig. 5). Very

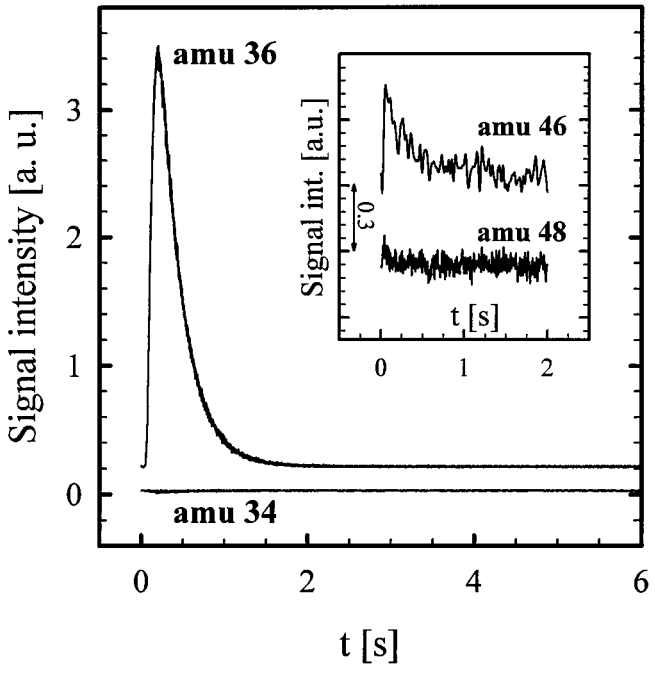

FIG. 5. Response signals for amu 36 ($^{18}O^{18}O$) and amu 34 ($^{18}O^{16}O$) upon a single pulse of isotope-labeled oxygen during CO oxidation in simulated methanol reformate over Au/α-Fe_2O_3 (75°C; vacuum flow mode). (Inset) Single pulse response for amu 46 ($C^{16}O^{18}O$) and amu 48 ($C^{18}O^{18}O$).

informative, however, are the results on isotope scrambling obtained from this experiment.

The first piece of information relates to adsorption and desorption of O_2. After pulsing isotope-labeled oxygen into the reaction mixture no oxygen scrambling,

$$^{36}O_2 + {}^{32}O_2 \leftrightarrow 2\,{}^{34}O_2, \qquad [1]$$

was observed for reaction temperatures between 75 and 100°C (CO conversion degrees between 15 and 25%), as would be expected for dissociative adsorption and subsequent recombinative desorption. This result fully agrees with the findings of Liu *et al.* on Au/TiO_2 (17) or Au/Fe_2O_3 (26). The experiment at 75°C is illustrated in Fig. 5. After subtracting the background signal caused by $^{16}O^{18}O$ impurities in the original isotope gas, there is no signal on amu 34 (= mixed product, $^{16}O^{18}O$) accompanying the $^{36}O_2$ pulse (amu 36). Consequently, oxygen either does not dissociate immediately after adsorption on the support (corresponding to the existence of molecular oxygen species) and/or the recombination/desorption step after dissociation is hindered by a high activation barrier, as would be characteristic for O_{ad} located on the gold particles (10).

Second, after a $^{36}O_2$ pulse, no doubly marked product, $C^{18}O^{18}O$ (amu 48), was observed (inset in Fig. 5). Due to the strong broadening of the CO_2 response by readsorption on the support material, however, the detection limit in such a single pulse experiment is relatively high. Therefore we admitted a series of 75 $^{36}O_2$ pulses to the gas feed (reactor temperature 75°C) at time intervals of 1 s, which is less than the decay time for the CO_2 signal after a single pulse. As a consequence, the response pulses overlap and add up, leading to an amplified signal, which in turn increases the experimental sensitivity drastically (Fig. 6). Still, no doubly marked product $C^{18}O^{18}O$ (amu 48) is found. This is in contrast to the experiments of Boccuzzi *et al.* over Au/ZnO and Au/TiO_2, who have reported the appearance of all possible products, $C^{16}O^{16}O$, $C^{16}O^{18}O$, $C^{18}O^{18}O$, and even $C^{18}O$, after reaction of $C^{16}O$ with $^{36}O_2$ (14, 43). These differences can be explained by effects related to CO_2 readsorption, which play an important role for conventional reactors but not in a TAP reactor experiment: In the first case this scrambling can result from the oxygen exchange of (re-)adsorbed CO_2 with the support, which according to Liu *et al.* occurs very fast for CO_2 (17). In the TAP reactor subsequent reactions of the product are of minor importance due to the much shorter contact times. Therefore the formation of doubly marked $C^{18}O^{18}O$, which was observed by Boccuzzi *et al.* in their *in situ* FTIR cell (14, 43) must be indeed attributed to a secondary reaction of the primary $C^{16}O^{18}O$ product, as was suggested in recent studies by Liu *et al.* (17, 26).

Finally, the absence of doubly marked CO_2 rules out any reaction scheme, which includes the direct reaction between molecular oxygen species and CO via a carbonate-like intermediate or transition state (pathway 2b in Fig. 1):

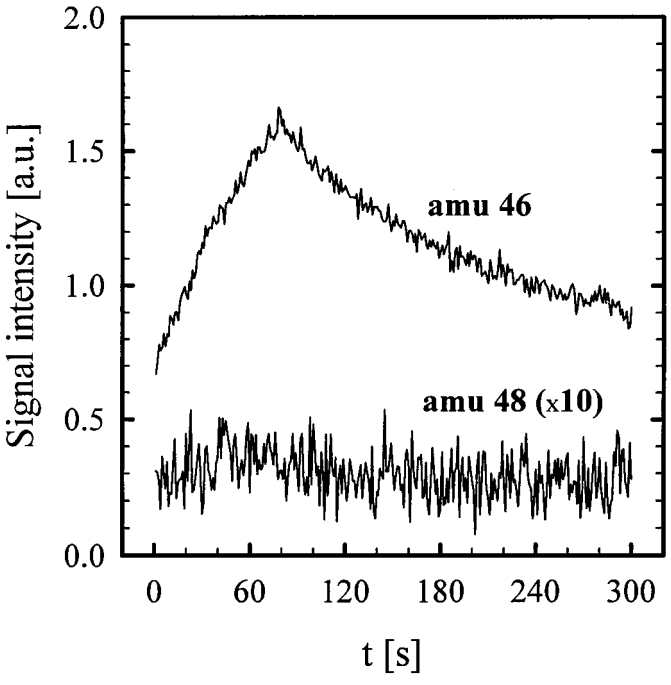

FIG. 6. CO_2-response signals for amu 46 ($C^{16}O^{18}O$) and amu 48 ($C^{18}O^{18}O$) for 75 subsequently admitted pulses (interval 1 s) of $^{36}O_2$ during CO oxidation in simulated methanol reformate over $Au/\alpha\text{-}Fe_2O_3$ (75°C; vacuum flow mode).

$$C^{16}O + {}^{36}O_2^- + e^- \leftrightarrow \left[\begin{array}{c} {}^{16}O \\ {}^{18}O \quad O^{18} \end{array}\right]^{2-}. \qquad [2]$$

For such a carbonate-like molecule, the cleavage of each oxygen bond in the following decomposition step, which yields CO_2, should have the same probability. This would lead to the formation of 33% doubly marked CO_2. On basis of a nonoccurring isotopic scrambling between $C^{18}O$ and the carbonate species observed in FT-IR experiments, Liu *et al.* came to similar conclusions and likewise excluded a successive reaction scheme via carbonate intermediates (17), as was previously proposed by Haruta *et al.* (16). Since a reaction of molecular oxygen species most likely would proceed via such a carbonate intermediate or transition state, the exclusion of the latter implies that a reaction scheme where the superoxide molecules dissociate at the metal–support interface in a first step, seems to be the most reasonable pathway (corresponding to pathway 2a in Fig. 1). In this picture, the molecularly adsorbed oxygen species act as a precursor species for the dissociative adsorption on gold and/or at the interface. The presence of adsorbed, most likely atomic (there is no evidence of an $O_{2,ad}$ species on Au at $T = 353$K), oxygen species on gold under reaction conditions is also indicated by our *in situ* DRIFTS measurements, where we noticed a significant blue shift (8 cm^{-1}) for preadsorbed CO upon the admission of

oxygen to the reaction cell (20), and which was similarly observed also by other groups (14, 19, 35, 44). Other explanations such as a support effect or interaction with oxygen on the support are highly unlikely since the C–O stretch vibration is in a very narrow frequency range for various Au catalysts as well as for massive Au samples (e.g., (5)) and since a similar effect is also observed for Au/Al_2O_3 (unpublished results), where oxygen adsorption under these conditions is only possible on the Au particles. Note that despite of the convincing evidence for the presence of O_{ad} on the gold particles a direct reaction between CO_{ad} and molecular oxygen species at the interface cannot be completely ruled out if other transition states than the symmetric, carbonate-like type are involved.

IV. CONCLUSIONS

The above and previous results lead to the following conclusions on the CO oxidation mechanism and on the role of the support on oxide supported Au catalysts:

- We suggested that metal oxide-supported Au catalysts can be grouped into two categories with respect to CO oxidation, which depend on the support material and differ also in the reaction mechanism: Gold catalysts with inert support materials, such as SiO_2, Al_2O_3, or MgO, are intrinsically less active. Catalysts with a relatively high activity can be prepared as well, but only if gold exists in a highly dispersed state. These catalysts show a strong dependence on the metal particle size and lose their activity rapidly with increasing size of the gold particles. For these systems we expect oxygen adsorption to occur directly on the gold particles, either on defect sites (steps, edges, and kinks) or facilitated by variations in the electronic structure of small metal particles.
- Au catalysts supported on reducible transition metal oxides such as Fe_2O_3 exhibit a significantly enhanced activity for CO oxidation, which is attributed to their ability to provide reactive oxygen. The existence of an oxygen reservoir on the support reduces the dependence of the turnover frequency on the gold particle diameter, since oxygen dissociation is no longer rate-limiting and, as a consequence, the TOF is not governed by particle size effects as were suggested for inert support materials. This, however, makes the performance probably sensitive toward the microcrystalline structure of the metal–support interface so that the activity of such systems often depends crucially upon the pretreatment method (see, e.g. (3, 45)). We postulate that the independence of the TOF from the Au particle size applies only to low metal loadings, where the metal particles are sufficiently distant from each other and the oxygen supply is not rate-limiting. (Note that the latter condition was not fulfilled in recent experiments on $Au/TiO_2(110)$ model systems, where such an independence was not observed (10, 21).)
- Oxygen adsorbs in large quantities on these "active" support materials in a molecular form, probably as a superoxide (O_2^-) species, as was proposed by Liu *et al.* (17). This explains the high surface mobility of adsorbed oxygen so that diffusion to the gold particles is not rate-limiting. Liu *et al.* suggested the adsorption to proceed on oxygen vacancies (17), which should be abundant in the vicinity of the gold clusters, due to the Schottky junction between the gold and the *n*-semiconducting support metal oxides (28).
- Dissociation of the molecularly adsorbed, mobile oxygen is suggested to take place at the metal–support interface, possibly followed by a spillover process of the atomic oxygen on the gold particles, before it reacts with CO_{ad} on the gold and/or at the interface (reaction scheme 2a in Fig. 1). Therefore, these molecular oxygen species may be described as a precursor species for the dissociative adsorption. The presence of atomic oxygen on the Au particles under reaction conditions is confirmed by the oxygen-induced blue shift in the C–O stretch vibration in our DRIFTS experiments (20).
- A direct reaction of CO_{ad} with molecular oxygen species involving a carbonate-like intermediate or transition state can be ruled out by the absence of doubly marked CO_2 product in our isotope studies. However, a reaction scheme including molecular oxygen cannot be generally excluded, if other configurations for the transition state are involved.

The mechanistic ideas proposed above explain well both the systematic differences in activity toward CO oxidation between Au catalysts supported on different oxides as well as the pronounced differences when compared to gold single crystals, where the reaction is blocked by the large activation barrier for oxygen dissociation. Further experiments are required, however, to unambiguously resolve the nature of the adsorbed molecular oxygen species on the support and the exact site and mechanism for oxygen dissociation.

ACKNOWLEDGMENTS

We thank J.-D. Grunwaldt (Haldor Topsoe) for helpful discussions. Financial support for this work came from the state Baden-Württemberg via the "Zukunftsoffensive Junge Generation." We are also grateful for a fellowship by the Deutsche Forschungsgemeinschaft for MMS, within the Graduiertenkolleg "Molekulare Organisation und Dynamik an Grenz- und Obeächen."

REFERENCES

1. Bond, G. C., and Thompson, D., *Catal. Rev. Sci. Eng.* **41**, 319 (1999).
2. Haruta, M., *Catal. Surv. Jpn.* **1**, 61 (1997).
3. Lin, S. D., Bollinger, M. A., and Vannice, M. A., *Catal. Lett.* **17**, 245 (1993).
4. Kahlich, M. J., Gasteiger, H. A., and Behm, R. J., *J. Catal.* **182**, 430 (1999).
5. Ruggiero, C., and Hollins, P., *Chem. Soc. Faraday Trans.* **92**, 4829 (1996).

6. Iizuka, Y., Fujiki, H., Yamauchi, N., Chijiiwa, T., Arai, S., Tsubota, S., and Haruta, M., *Catal. Today* **36**, 115 (1997).
7. Canning, N. D. S., Outka, D. A., and Madix, R. J., *Surf. Sci.* **141**, 240 (1984).
8. Hammer, B., and Nørskov, J. K., *Nature* **376**, 238 (1995).
9. Parker, D. H., and Koel, B. E., *J. Vac. Sci. Technol. A* **8** (3) 2585 (1990).
10. Bondzie, V. A., Parker, S. C., and Campbell, C. T., *J. Vac. Sci. Technol. A* **17**, 1717 (1999).
11. Parker, D. H., Fischer, D. A., Colbert, J., Koel, B. E., and Gland, J. L., *Surf. Sci. Lett.* **236**, L372–L376 (1990).
12. Gottfried, J. M., Schmidt, K. J., Christmann, K., and Schroeder, S. L. M., *Surf. Sci.*, in preparation.
13. France, J., and Hollins, P., *J. Electr. Spectr. Rel. Phenom*. **64/65**, 251 (1993).
14. Boccuzzi, F., Chiorino, A., Tsubota, S., and Haruta, M., *J. Phys. Chem*. **100**, 3625 (1996).
15. Grunwaldt, J.-D., and Baiker, A., *J. Phys. Chem*. **103**, 1002 (1999).
16. Haruta, M., Tsubota, S., Kobayashi, T., Kageyama, H., Genet, M. J., and Delmon, B., *J. Catal.* **144**, 175 (1993).
17. Liu, H., Kozlov, A. I., Kozlova, A. P., Shido, T., Asakura, K., and Iwasawa, Y., *J. Catal.* **185**, 252 (1999).
18. Bollinger, M. A., and Vannice, M. A., *Appl. Catal. B* **8**, 417 (1996).
19. Tripathi, A. K., Kamble, V. S., and Gupta, N. M., *J. Catal.* **187**, 332 (1999).
20. Schubert, M. M., Kahlich, M. J., Gasteiger, H. A., and Behm, R. J., *J. Power Sources* **84**, 175 (1999).
21. Valden, M., Pak, S., Lai, X., and Goodman, D. W., *Catal. Lett.* **56**, 7 (1998).
22. Haruta, M., *Catal. Today* **36**, 153 (1997).
23. Mavrikakis, M., Stoltze, P., and Nørskov, J. K., *Catal. Lett.* **64**, 101 (2000).
24. Kozlov, A. I., Kozlova, A. P., Liu, H., and Iwasawa, Y., *Appl. Catal. A* **182**, 9 (1999).
25. Fukushima, K., Takaoka, G. H., Matsuo, J., and Yamada, I., *Jpn. J. Appl. Phys.* **36**, 813 (1997).
26. Liu, H., Kozlov, A. I., Kozlova, A. P., Shido, T., and Iwasawa, Y., *Phys. Chem. Chem. Phys.* **1**, 2851 (1999).
27. Richardson, J. T., "Principles of Catalyst Development." Plenum Press, New York, 1992.
28. Frost, J. C., *Nature* **18**, 577 (1988).
29. Andreeva, D., Idakiev, V., Tabakova, T., Andreev, A., and Giovanoli, R., *Appl. Catal. A* **134**, 275 (1996).
30. Schubert, M. M., dissertation, University of Ulm, 2000.
31. Gleaves, J. T., Ebner, J. R., and Kuechler, T. C., *Catal. Rev. Sci. Eng.* **30**, 49 (1988).
32. Grunwaldt, J.-D., Kiener, C., Wögerbauer, C., and Baiker, A., *J. Catal.* **181**, 223 (1999).
33. Okumura, M., Nakamura, S., Tsubota, S., Nakamura, T., Azuma, M., and Haruta, M., *Catal. Lett.* **51**, 53 (1998).
34. Cunningham, D. A. H., Vogel, W., Kageyama, H., Tsubota, S., and Haruta, M., *J. Catal.* **177**, 1 (1998).
35. Grunwaldt, J.-D., Maciejewski, M., Becker, O. S., Fabrizioli, P., and Baiker, A., *J. Catal.* **186**, 458 (1999).
36. Schubert, M. M., Plzak, V., Garche, J., and Behm, R. J., in preparation.
37. Shen, J., Guang, B., Tu, M., and Chen, Y., *Catal. Today* **30**, 77 (1996).
38. Olowe, A., *Adv. X-Ray Anal.* **38**, 749 (1995).
39. Grass, K., and Lintz, H.-G., *J. Catal.* **172**, 446 (1997).
40. Kahlich, M. J., Gasteiger, H. A., and Behm, R. J., *J. New Mater. Electrochem. Systems* **1**, 39 (1998).
41. Li, Y.-E., Boecker, D., and Gonzalez, R. D., *J. Catal.* **110**, 319 (1988).
42. Kahlich, M. J., Schubert, M. M., Hüttner, M., Noeske, M., Gasteiger, H. A., and Behm, R. J., *in* "New Materials for Fuel Cells and Modern Battery Systems II" (O. Savadogo and P. R. Roberge, Eds.), p. 642. Ecole Polytechnique de Montreal, Montreal, 1997.
43. Boccuzzi, F., Chiorino, A., Tsubota, S., and Haruta, M., *Catal. Lett.* **29**, 225 (1994).
44. Boccuzzi, F., Chiorino, A., Manzoli, M., Andreeva, D., and Tabakova, T., *J. Catal.* **188**, 176 (1999).
45. Kang, Y.-M., and Wan, B.-Z., *Catal. Today* **26**, 59 (1995).
46. Park, E. D., and Lee, J. S., *J. Catal.* **186**, 1 (1999).
47. Yuan, Y., Asakura, K., Wan, H., Tsai, K., and Iwasawa, Y., *Catal. Lett.* **42**, 15 (1996).
48. Yuan, Y., Asakura, K., Kozlova, A. P., Wan, H., Tsai, K., and Iwasawa, Y., *Catal. Today* **44**, 333 (1998).
49. Haruta, M., Kageyama, H., Kamijo, N., Kobayashi, T., and Delannay, F., *in* "Successful Design of Catalysts" (T. Invi, Ed.), p. 33. Elsevier, Amsterdam, 1988.